Photoluminescence, structural, morphology and dielectric properties of $BaTi_{0.9}Sn_{0.1}O_3$ doped with Nd^{3+} and Nd^{3+}/ Yb^{3+} ions

O. El-sayed [a], W. M. Mousa [a], Safaa K. El-Mahy [a], M. A. Salem [b], I. K. Battisha[b], Ragab. Mahani[c], A. lahmar[d], M. El Marssi[d]

[a]Physics Department, Girls College for Arts, Science and Education, Ain Shams University, Cairo, Egypt

[b]Solid State Physics Department, Physics Research Division, National Research Centre, Dokki, Giza 12622, Egypt (Affiliation ID: 60014618)

[c]Microwave Physics and Dielectrics Department, National Research Centre, Dokki, Giza 12622, Egypt (Affiliation ID: 60014618)

[d]LPMC, Université de Picardie Jules Verne, 33 rue Saint-Leu, 80039 Amiens Cédex, France

Abstract

Nano-structure $BaTi_{0.9}Sn_{0.1}O_3$ (BTSO) doped with Nd^{3+} (BTSO: 5N) and co-doped with Nd^{3+}/Yb^{3+} ions (BTSO: 5NY), were prepared using the modified sol-gel method in powder form and annealed at 1050^{o}C in air for 4h. Their structural, morphological, photoluminescence and dielectric properties studies were investigated. The crystallite sizes from XRD and TEM found to be decreased upon doping with $Nd^{3+}$and Nd^{3+}/Yb^{3+} ions, respectively. FTIR results showed enhancement of crystallinity and absence of carbonates upon increasing Yb^{3+} ions. TEM micrographs show that particles have spherical shape with small size within the nano-structure phase. FESEM microphotographs showed a density increase due to replacement of $Nd^{3+}$and Yb^{3+}ions at the B-site (Ti^{4+}). From photoluminescence it was obtained that emissivity quenched by increasing Yb^{3+} ions concentration as the Nd^{3+} act as sensitizer for Yb^{3+}. Cuire temperature (T_c) of doped and co-doped samples shifted to lower values. Besides, their permittivity and AC conductivity increased in comparison with BTSO.

Keywords: BTSO, XRD, Curie temperature, dielectric properties

***Corresponding author:** olfat_elsayed2009@yahoo.com

1. Introduction

Rare earth (RE) doped oxide materials are investigated extensively due to their wide range of interesting applications from solid state lighting, fiber-optic communication, LEDs,

display devices, to therapeutic and biomedical applications [W. Yang et al. 2014, Z. Gu et al. 2013, H. Lian et al. 2013]. With the extensively developments in nanotechnology and chemical synthesis processes, a grating interest is noticed to achieve control over the structures and morphology of the oxide phosphor materials in order to optimize the luminescence emission efficiency with respect to specific technology requirements [F. Wang et al. 2009].

Moreover, the motivations of researchers to think on multifunctional and hybrid materials is the public need of cheap and reliable multitasking materials. In fact known that the rare earth ions (RE) show luminescence not only down conversion (Stokes type) but also up conversion (anti-Stokes type) and the superiority of the latter one is already well established [F. Auzel et al. 2004]. The up-conversion (UC) process from near-infrared to visible is an important approach for a generation of visible luminescence and short wavelength laser actions. Recently, the interest in up-conversion emission has been increased due to the needs for all-solid compact laser devices operating in the blue-green region and the availability of near infrared powerful GaAs/(Al, Ga) as laser diodes that can be used in such systems[I. K. Battisha et al. 2010]. The conversion process requires the participation of a luminescent material having multiple energy levels with appropriate energy spacing. In this respect, lanthanide ions offer interesting features for UC materials, since 4f shell range from the near infrared to the ultraviolet part of the electromagnetic spectrum.

In all oxide compounds, Ln^{3+} ions are expected to occupy the A-site of the perovskite (ABO_3) lattice due to their ionic size and the excess positive charge must be compensated. However, it is also possible to replace some of the B- site by Ln^{3+} with keeping the overall charge neutrality. From the previously reported on Ln^{3+} ions, the effects of RE^{3+} substitution on the luminescent $BaTiO_3$, We observed that the RE^{3+} cations replace the B^{4+} ions at low concentrations, when its concentration increased both, A^{2+} and B^{4+} ions, are replaced [S. Fuentes et al. 2013].

The objective of this work is to study the structural, morphology, photoluminescence and dielectric properties of $BaTiSnO_3$:co-doped with Nd^{3+} and Nd^{3+}/Yb^{3+}ions, prepared by the modified sol – gel method and annealed at 1050^{o}C in air for 4h. XRD, FTIR, TEM, FESEM techniques were used to evaluate the structural and morphological features of the particles. Dielectric properties were investigated by means dielectric spectrometer over a wide frequency range (10^1 - 10^6 Hz) at different temperatures. The dielectric permittivity curves are new and also the phase transition and Curie temperature are not famous for such RE^{3+} ions doping $BaTiSnO_3$.

2. Experimental work

2.1 Synthesis

The chemical reagents used for preparation BTSO, BTSO: 0.5 mol % Nd and BTSO: 5Nd/(0.75, 1) mol % Yb) ceramics, are barium acetate $Ba(CH_3COO)_2$, titanium (IV) n-butoxide$Ti(OC_4H_9)_4$, tin chloride $SnCl_4.5H_2O$, neodymium nitrate $Nd(NO_3)_3.6H_2O$ and ytterbium nitrate $Yb(NO_3)_3{\cdot}5H_2O$, as sources of Ba^{2+}, Ti^{4+}, Sn^{4+}, Nd^{3+} and Yb^{3+} ions as the starting precursors, respectively. The purity and molecular weight of these reagents were listed in Table 1. Acetyl acetone $C_5H_8O_2$ and acetic acid ($C_2H_4O_2$) diluted with distilled water (HAc)–H_2O were selected as solvents of titanium (IV) n-butoxide and barium acetate, respectively. Barium titanate (BTO) was obtained by reacting two solutions of barium acetate and titanium (IV) n-butoxide stirred for 1h(Sol.1). Solution of respective amount of $SnCl_4.5H_2O$ dissolved in 16 ml isopropanol stirred for 15 min (Sol.2). Sol.2 was added to Sol.1 and stirred for another 15 min and dried and annealed then BTSO was obtained. The solution of 0.5 mol % of Nd $(NO_3)_3.6H_2O$ dissolved in 5ml of (HAc)–H_2O (Sol.3) was added to (Sol.2) and stirred for 45 min. For Nd^{3+}/Yb^{3+} Co-doped samples, $Yb(NO_3)_3{\cdot}5H_2O$ dissolved in 5ml of (HAc)–H_2O(Sol.4). Sol.4 was added to Sol.3 then added toSol.2, the mixture stirred for 45 min. Gel was formed at ~ 130^{o}C and densification of gel was carried out by annealing in air for 4 h at 1050^{o}C. Muffle furnace type Carbolite CWF1200 was used for samples annealing. The chemical formula and sample abbreviation are listed in Table2.

Table. 1. The compound, chemical form, molecular weight and purity of used materials.

Compound	Chemical form	Molecular weight	Purity %	Company
Barium acetate	$Ba(CH_3COO)_2$	255.42	99	Sisco Research Laboratories PVT.LTD, India
Acetic acid	$C_2H_4O_2$	60.06	99.5	Adwic, Egypt
Titanium(IV)n-butoxide	$Ti(C_4H_9O)_4$	340.35	98+	Sigma–Aldrich, Germany
Acetyl acetone	$C_5H_8O_2$	100.12	≥98	Fluka, Switzerland
Tin(IV) chloride pentahydrate	$SnCl_4.5H_2O$	350.60	98	Strem Chemicals, Incorporated
Isopropanol	C_3H_8O	60.02	99	Adwic, Egypt
Neodmium nitrate hexahydrate	$Nd(NO_3)_3.6H_2O$	438.35	99.9	Sigma–Aldrich, Germany
Ytterbium nitrate pentahydrate	$Yb(NO_3)_3.5H_2O$	449.13	99.9	Sigma–Aldrich, Germany

Table. 2 Dopant name, dopant concentration, sample abbreviation, chemical formula of BTSO ceramics

Dopant name	Dopant concent. (mol%)	Sample abbreviation	Chemical formula
Without	0.0	BTSO	$BaTi_{0.9}Sn_{0.1}O_3$
Nd^{3+}	0.5	BTSO: 5N	$BaTi_{0.895}Sn_{0.1}Nd_{0.005}O_3$
Nd^{3+} /Yb^{3+}	0.5/0.75	BTSO: 5N7Y	$BaTi_{0.8875}Sn_{0.1}Nd_{0.005}Yb_{0.0075}O_3$
Nd^{3+}/Yb^{3+}	0.5/1	BTSO: 5N1Y	$BaTi_{0.885}Sn_{0.1}Nd_{0.005}Yb_{0.01}O_3$

2.2 Characterization

Philips X-ray diffractometer (XRD) with mono-chromatized $CuK_{\alpha 1}$ (λ= 1.5406 Å), was used for characterizing the crystalline structure of all samples. The crystallite size (C_s) calculated from the Scherrer's equation [P. Klugp et al. 1954];

$$C_s = K\lambda / B\cos\theta \qquad (1)$$

Where, K (= 0.89) is Scherer constant, λ is the wavelength, B is the full width of the peak at half maximum (FWHM) intensity (in radians) and θ is the diffracted angle.

The chemical structure and function groups of samples were characterized using Fourier Transform InFrared (FTIR) spectroscopy (thermo Nicolet, FT-IR and NEXUS in the range from 4000 up to 400 cm^{-1}.

The transmission electron microscope (TEM) using a JEOL JEM-1230 equipment operating at 120 kV with attached CCD camera. Field emission scanning electron microscopy (FESEM) with energy dispersive X-ray (EDX) analysis provided with variable pressure FESEM instrument (FEI, model: Quanta 250 FEG).

Photoluminescence emissivity was measured using spectrofluorometer model Jasco FP-6500 Japan. The light source used is Xenon arc lamp 150 watt; the excitation monochrometer and emission monochrometer have width of 5nm. All measurements done at room temperature and at the same geometrical conditions.

The dielectric properties measured over a wide frequency range (10^2 - 10^6 Hz) at different temperatures in the range between (-100-150) ^oC, and using a computerized Impedance Analyzer (IM3570). The dielectric properties such as the permittivity (ε') and alternative current conductivity AC (σ_{ac}) are calculated from the output parameters such as capacitance (C) and loss tangent ($tan\delta$) as follows:

$$\varepsilon' = \frac{Cd}{\varepsilon_o A} \qquad (2)$$

$$\sigma_{ac} = \omega \varepsilon_o \varepsilon' tan\delta \qquad (3)$$

Where ε_o is the permittivity of free space (8.854 x 10^{-12} F/m), ω (= $2\pi f$) is the angular frequency of the applied electric field in Hertz, d is the sample thickness and A is the sample surface area subjected to the electric field.

3. Results and discussion

3.1. X-Ray Diffraction

Fig.1. shows the XRD patterns of (BTSO), BTSO: 5N, BTSO: 5N7Y and BTSO: 5N1Y powders annealed at 1050°C for 4h in air. From the Fig1.a the principle peak appeared at $2\theta=31.51^{o}$ dictated the tetragonal phase presence [Q. Sun et al. 2017]. The XRD data for all samples completely matched with the tetragonal ICDD card no [74-2491]. As shown in Fig.1a undesirable traces of SnO_2 appeared in all samples, its intensity decreased by increasing doping concentration. It is clear that in Nd^{3+} and Nd^{3+}/Yb^{3+}ions Co-doped samples there is no obvious secondary phase appeared, referring to Nd^{3+} and/ orYb^{3+}ions, so these ions are completely embedded in the BTSO crystal lattice. The general detected behavior from the values of the crystallite sizes and intensities change of the peaks by doping with 0.5 mol % of Nd^{3+} ions, where it shifts the principle peak to lower $2\theta^{o}$ and decrease tetragonality than of BTSO. Moreover co-doped Yb^{+3} ions cause the same mentioned action of Nd^{3+} ions and introduce significant changes in the crystalline lattice due to substitution of Ti^{4+} with Nd^{3+} and $Yb^{+3}$of larger ionic radii [A. P. A. Moraes et al. 2011] as shown in Fig.1. (a). and Table.3.

Fig.1. (b) shows the expansion XRD patterns over a $2\theta^{o}$ range between44 and 46^{o}, peaks splitting around 45° are indicated to BTSO, BTSO: 5N, BTSO: 5N7Y, BTSO: 5N1Y, Perovskite tetragonal phase presence, which decreased by increasing the Yb^{3+} ions concentration from 0.75 up to 1 mol %, and shifted to lower $2\theta^{o}$ values. These results showed change in the lattice parameter (a, c) values with also tetragonality as seen in Table.3. It is also seen from Table3., that the crystallite size decreases by RE^{3+}doping, this may be due to the fact that the substitution of Ti^{4+} ions with larger ionic radius of Nd^{3+} and Yb^{3+} ions cause It's internal stress in the crystal which increases by increasing Yb^{+3} ions concentration [30].
[Y. Li et al .2016,].

Table.3. Samble abbreviation Calculated lattice parameter, tetragonal factor (c/a), crystallite size (C. S), structure and Particle size (P.S) of BTSO, BTSO: 5N, BTSO: 5N7Y and BTSO: 5N1Y samples annealed at 1050^{o}C.

Samble abbreviation	Lattice parameter		Tetragonal factor (c/a)	C. S (nm) From XRD	Structure	P.S (nm) From TEM
	a,b (A°)	c (A°)				
BTSO	3.9924	4.0130	1.0051	42	Tetragonal	47
BTSO: 5N	3.9933	4.0125	1.0048	39.57	Tetragonal	44.33
BTSO: 5N /7Y	4.0003	4.0109	1.0026	37	Tetragonal	-
BTSO: 5N /1Y	4.0032	4.0093	1.0015	34.68	Pseudo cubic	-

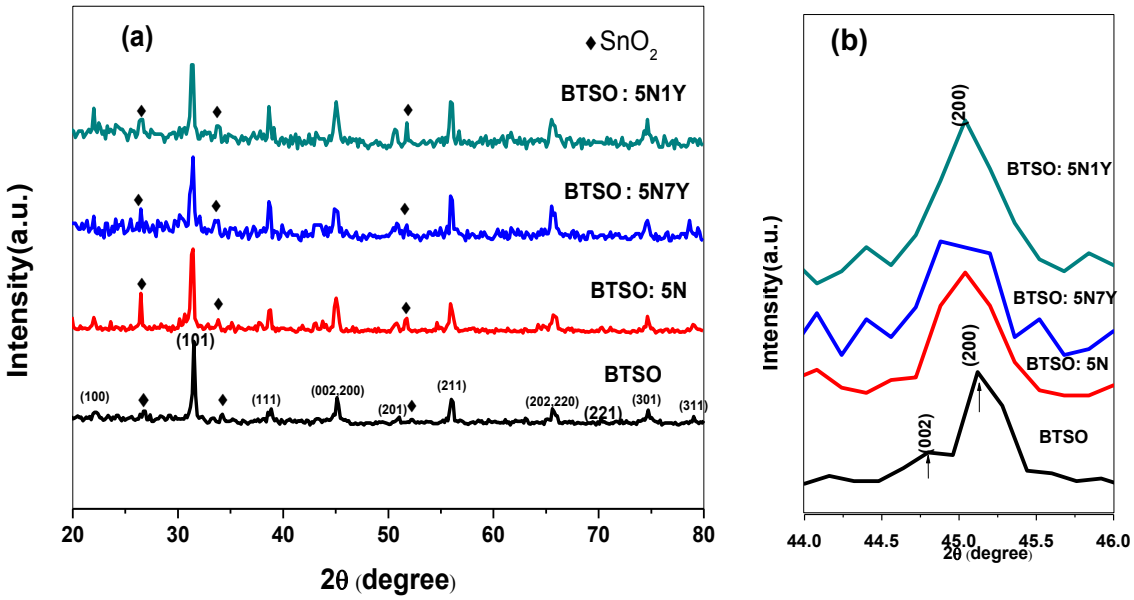

Fig.1. XRD patterns of BTSO, BTSO: 5N, BTSO: 5N7Y and BTSO: 5N1Y (a), 2θ^o extending area between =44 and 46^o (b) for all samples.

3.2. FTIR Analysis

FTIR spectra of BTSO, BTSO: 5N, BTSO: 5N7Y and BTSO: 5N1Y are shown in Fig. 2. From the spectrum of BTSO the absorption bands at 430 cm^{-1} and 854cm^{-1}, confirming the perovskite structure of sample. Also the band at 430 cm^{-1} is allocated to the bending vibrations of the M-O bond in the tetrahedral site and the band at 854 cm^{-1} is allocated to control of metal-oxygen stretching vibrations results from tetrahedral sites and oxygen complexes [G. R. Gajula et al. 2019]. In addition to these bands there is more bands was observed at 566 and 680 cm^{-1} also assigned to M-O stretching vibration along the polar axis of spontaneous polarization was found also in BTO_3 tetragonal phase as previously reported [G. R. Gajula et al. 2019, T. Tunkasiri et al. 1994, W. Thandar et al. 2008 and E. Chavez et al 2010]. The bands at 430, 566 and 680 cm^{-1} in the spectrum of BTSO shifted to lower wavenumber by increasing the RE^{3+} doping concentration. The difference appeared in band

positions are caused by different lengths, strengths, and effective mass of the metal oxygen bonds, were Sn, Nd, Yb in B sites of $BaTiO_3$ tetragonal structure [C. M. B Henderson et al. 1997, D. M. Sherman. 1984 and A. B. Gadkari et al. 2009].

The bands assigned to vibration of carbonate group (CO_3^{2-}) appeared at 1024 and 1386 cm^{-1} [W. Thandar et al. 2008], these bands decreases in intensity by increasing RE^{3+} ions concentration, also the band at 1386 cm^{-1} is shifted to 1435 cm^{-1} in pure BTO_3 [S. Wei Lu et al. 2000], the obtained results are in combatable with the previously reported by [S. Tangwiwat et 2005] who suggested that band at 1435 cm^{-1} is assigned to lattice carbonate moreover due to its higher sensitivity

The band at 1627 cm^{-1} is due to the decomposition mode of the absorbed H_2O molecules, attributed to O-H bending vibration [W. Thandar et al. 2008], while the band at 3438 cm^{-1} are assigned to O-H stretching modes of surface adsorbed water . Nd^{3+} and Yb^{3+} co-doped samples are showing two bands around 1627and 3438 cm^{-1} which shifts to lower wavenumbers and decreases in intensity, moreover it become more broad by increasing Yb^{3+} concentration, which appeared due to the formation of molecular water [I. K. Battisha et al. 2006]. There was a co-existence of OH stretching at 3438cm^{-1} with the carbonate absorptions at1386 cm^{-1}, suggesting that the carbonate may be in the form of a hydroxy carbonate. The very weak band at 2927 cm^{-1} assigned to C-H stretching vibrations of CH_3, its intensity broad and can be negligible for RE^{3+}doped samples.

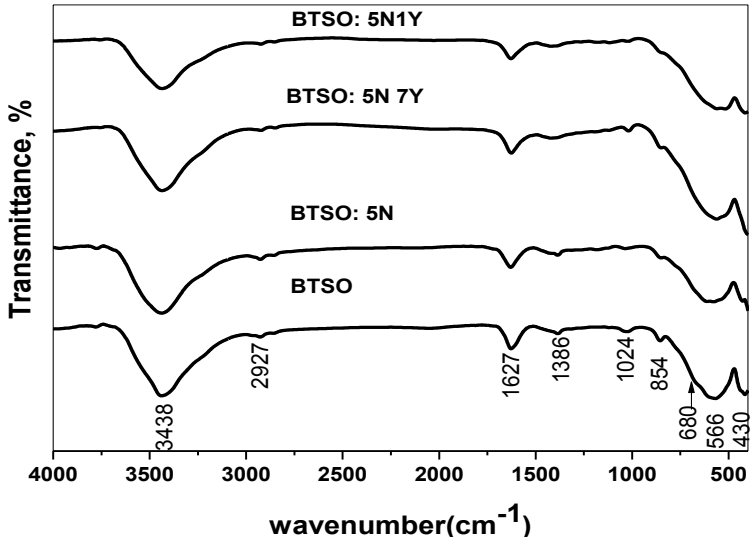

Fig.2. FTIR spectra of BTSO, BTSO: 5N, BTSO: 5N7Y, BTSO: 5N1Y annealed at 1050°C for 4 h in air.

3.3. Transmission electron microscope (TEM) analysis

Figs.3a and b shows the representative TEM micrographs selected samples for BTSO and BTSO: 5N, respectively. From the figures, it is clear that Some degree of agglomerations has been found in the clusters, which contain many small grains, with some particles have clear tetragonal shape in dispersed regions which becomes more clearly for BTSO: 5N (Fig. 3b) confirming higher crystallinity of samples [Q. Sun et al. 2017], it is also obtained that the paricle size increases from 41 to 45 nm by doping which is in good accordance to XRD results as listed in Table .3.

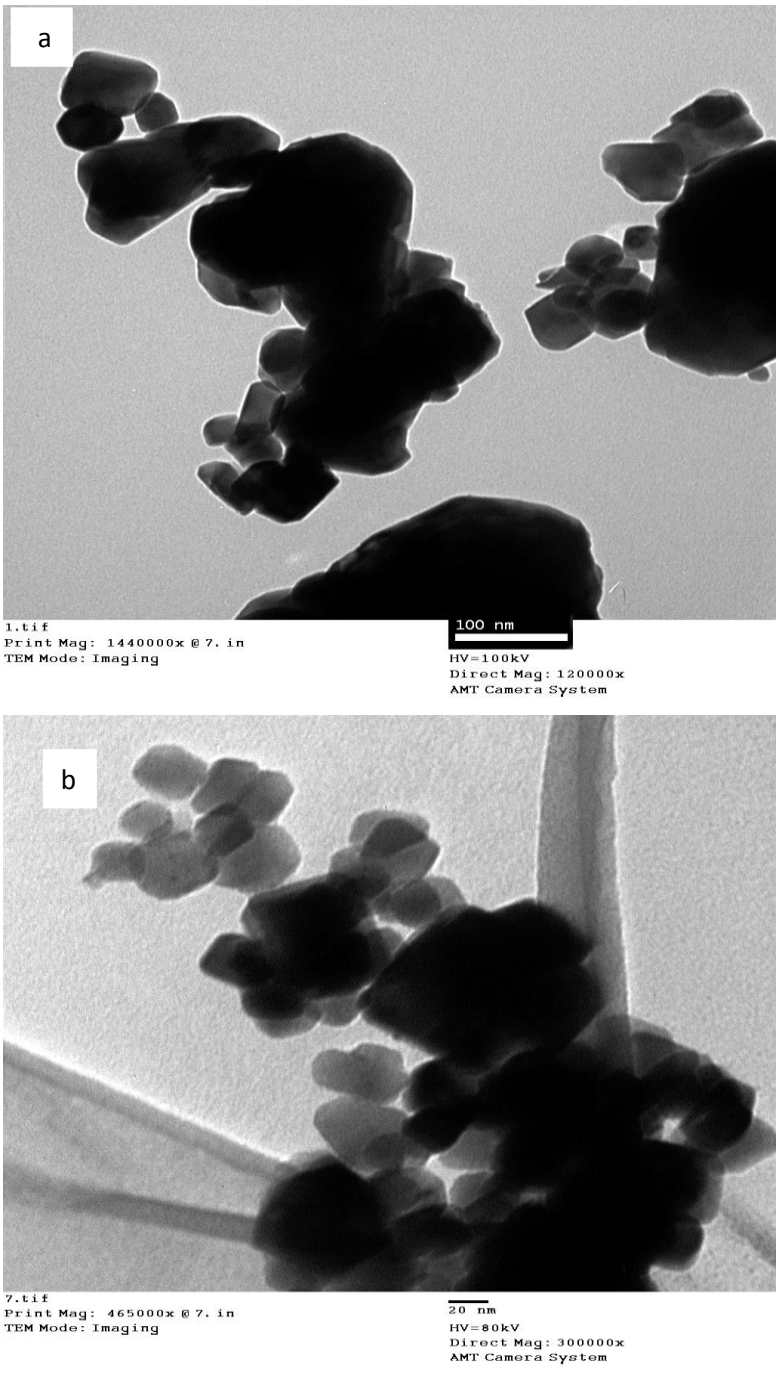

Fig. 3. TEM micrograph of BTSO (a) and BTSO: 5N (b) samples respectively, annealed in air for 4 h at 1050^{o}C

3.4. Field Emission Scanning electron microscope (FESEM) characterization

Fig.4 shows the field emission scanning electron micrographs (FESEM) for BTSO, BTSO: 5N, BTSO: 5N7Y and BTSO: 5N1Y. For all the samples, the morphological shape of the particles was irregular; containing some also larger grains due to replacement of Ti^{4+} with Nd^{3+} and Yb^{3+}ions of larger ionic radius [H. C. R. Bitra et al. 2014], the particles are nearly tetragonal in nature and agglomerated due to the higher annealing temperature. The tetragonality decreased with Nd^{3+} ions doping and decreased more by co-doping with Yb^{3+} ions giving the shape is more spherical and higher density. The significant grain size increase as a result of doping in good agreement with the XRD results

Energy dispersive X-ray analysis (EDX) suggested the good formation of samples as shown in Fig. 5. It can notice that BTSO has high intensity peaks corresponding to oxygen, Ba,Ti and Sn elements, confirming the absence of any impurities Fig. 5 (a). Peaks with low intensities corresponding to Nd^{3+} ions observed in EDX due to its low concentration comparing to other mentioned elements Fig. 5 (b). The presence of Nd^{3+} and Yb^{3+} observed in EDX Fig. 5 (c, d) with low peak intensities also due to their lower concentrations.

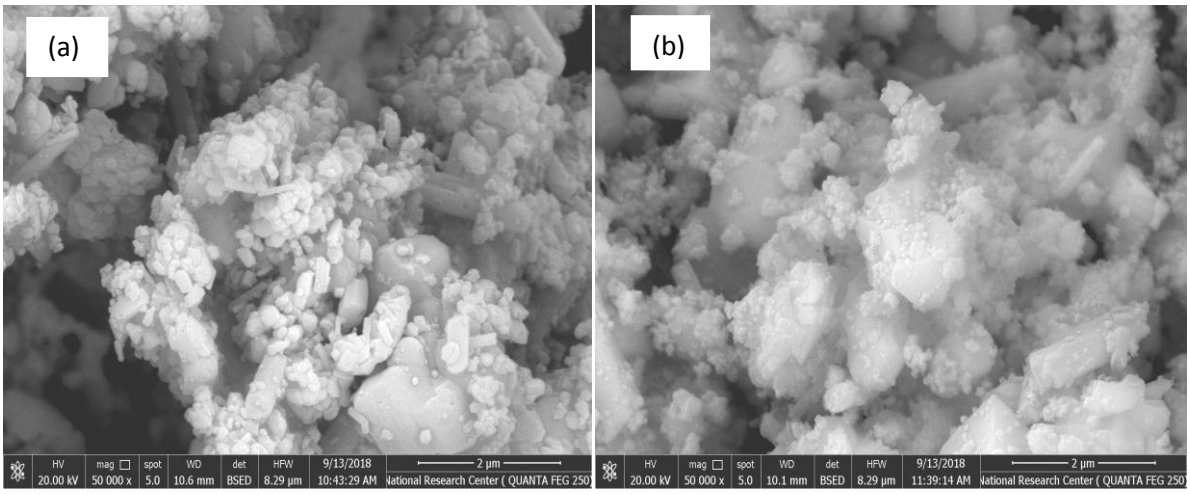

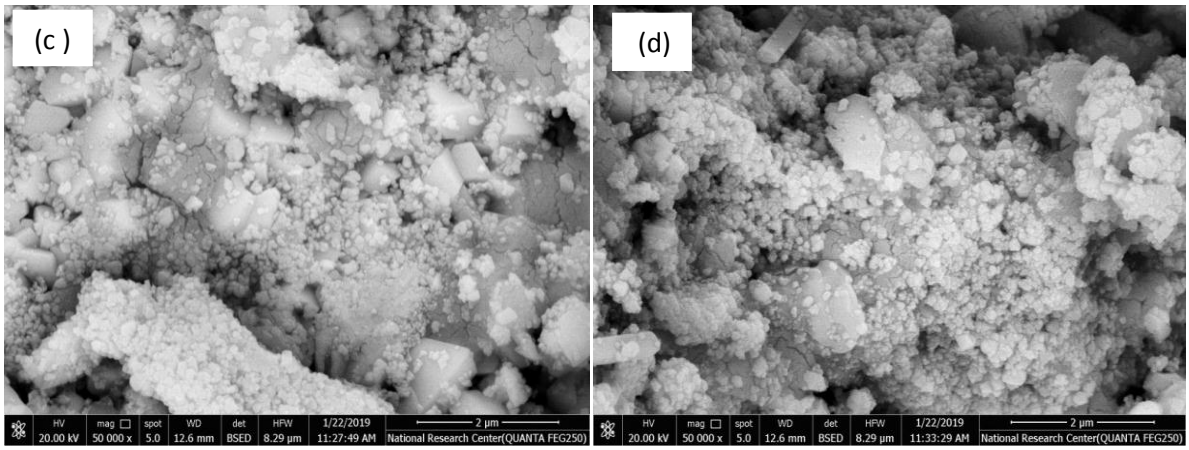

Fig. 4. FESEM micrograph of BTSO (a), BTSO: 5N(b), BTSO: 5N7Y (c) BTSO: 5N1Y (d)samples, annealed in air for 4h at 1050^{o}C

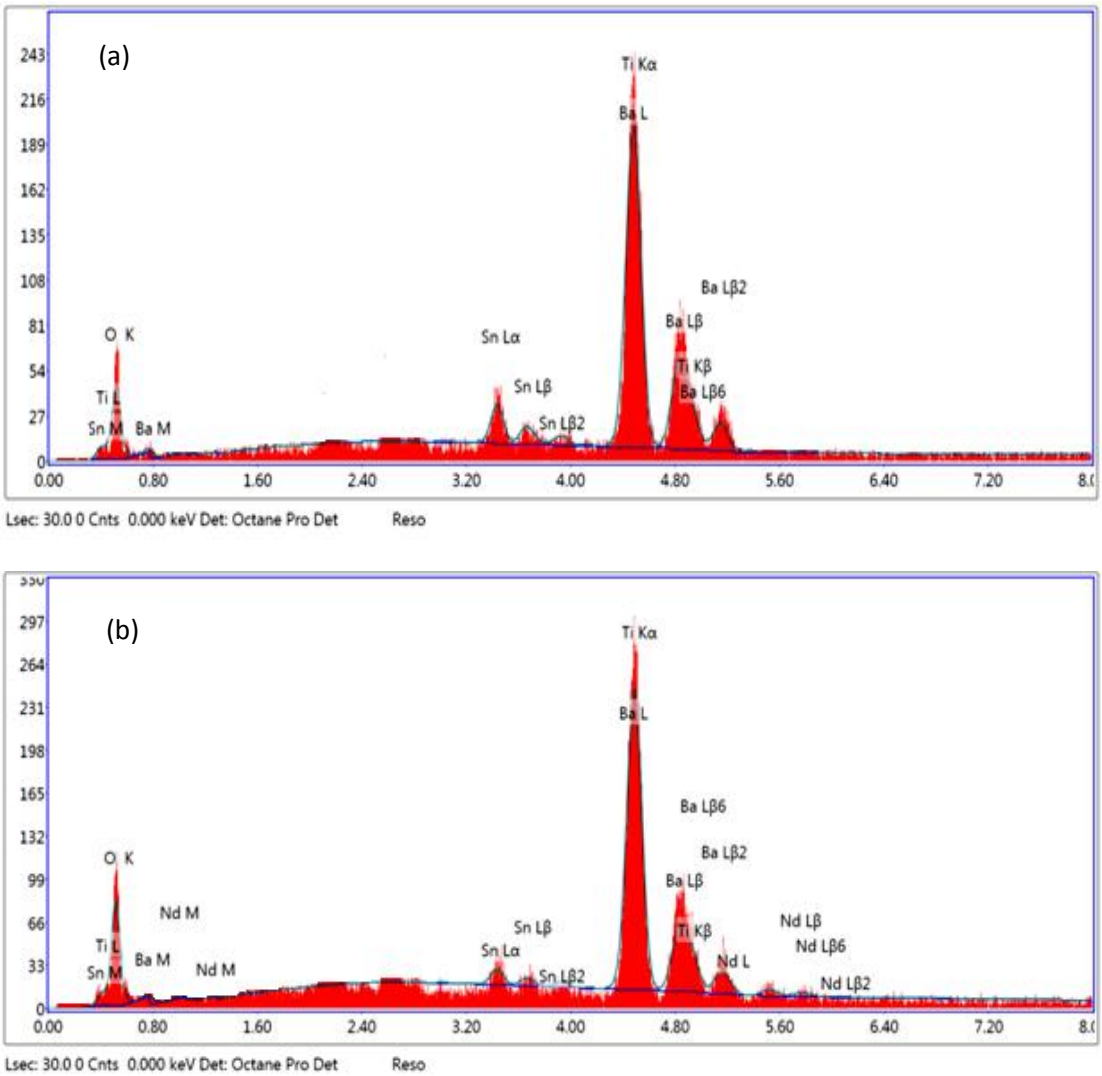

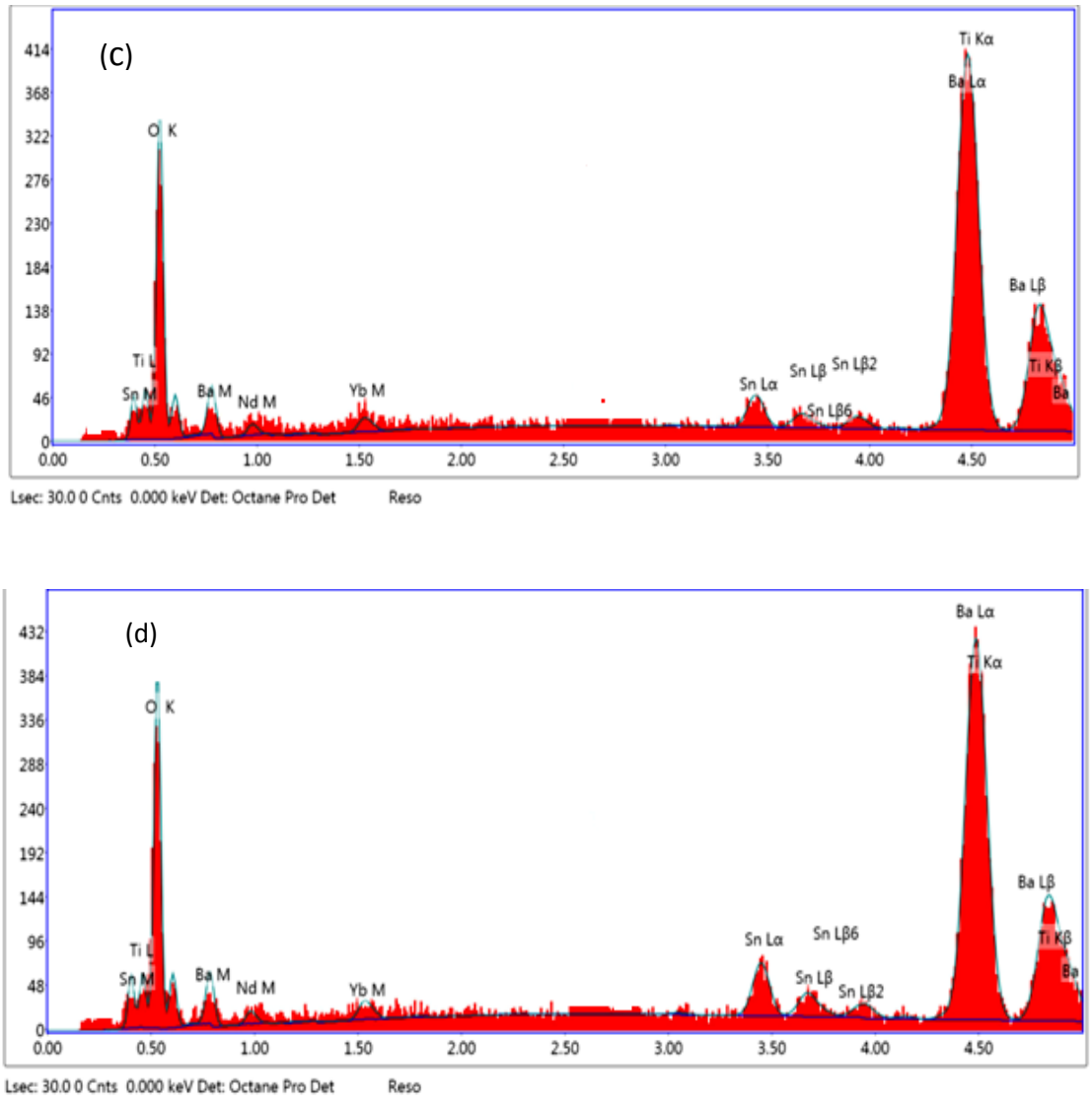

Fig. 5. EDX image of BTSO (a), BTSO: 5N (b), BTSO: 5N7Y (c) BTSO: 5N1Y (d)samples, annealed in air for 4 h at 1050^{o}C

3.5. Up conversion Emission

Fig.6. Shows the up-conversion spectra for BTSO: 5N, BTSO: 5N7Y and BTSO: 5N1Yannealed in air for 4h at 1050°C, were excitated with 900 nm at room temperature. All the spectra consist of characteristic bands, ascribed to the electronic transitions of Nd^{3+} ions, basically on the established energetic model [W. T. Carnall et al. 1975].

It is clearly visible that the most intense emission corresponds to the emission band at 592 and assigned to the ($^4G_{5/2}+^2G_{7/2}\rightarrow{}^4I_{9/2}$), green emission, the group band at 611, 646 and 690 nm resulted in red emission, were band at 611 nm assigned to ($^2H_{11/2}\rightarrow{}^4I_{9/2}$) and group emission bands at 646 and 690 nm assigned to ($^4F_{9/2}\rightarrow{}^4I_{9/2}$). Another group emission bands attributed to Infrared emission at 710, 730, 764, 824 and 883 nm are detected, where group

emission bands at 710, 730, 764 nm assigned to ($^4F_{7/2}$+$^4S_{3/2}$→$^4I_{9/2}$) and the two emission bands at 824 and 883 nm assigned to ($^4F_{5/2}$+ $^2H_{9/2}$→$^4I_{9/2}$) and ($^4F_{3/2}$→$^4I_{9/2}$) are observed.

It is also can notice from Fig. 6 that the emission line of Nd^{3+}/Yb^{3+} co-doped samples contain both the emission bands of Nd^{3+} and Yb^{3+}, but the emission of Nd^{3+} is greatly quenched in the co-doped samples, which suggests that energy transfer from Nd^{3+} to Yb^{3+} is possible in this component [C.H. Yang et al. 2007].

That the UC emission intensity decreases with increasing Yb^{3+} ions concentration, this observation revealed the increase of energy transfer and non-radiative processes that compete with luminescence. The inset appeared in Fig.6. Shows a small little bit shift in peak position to lower wavelength value by increasing Yb^{3+} ions concentration, and a decrease in intensity.

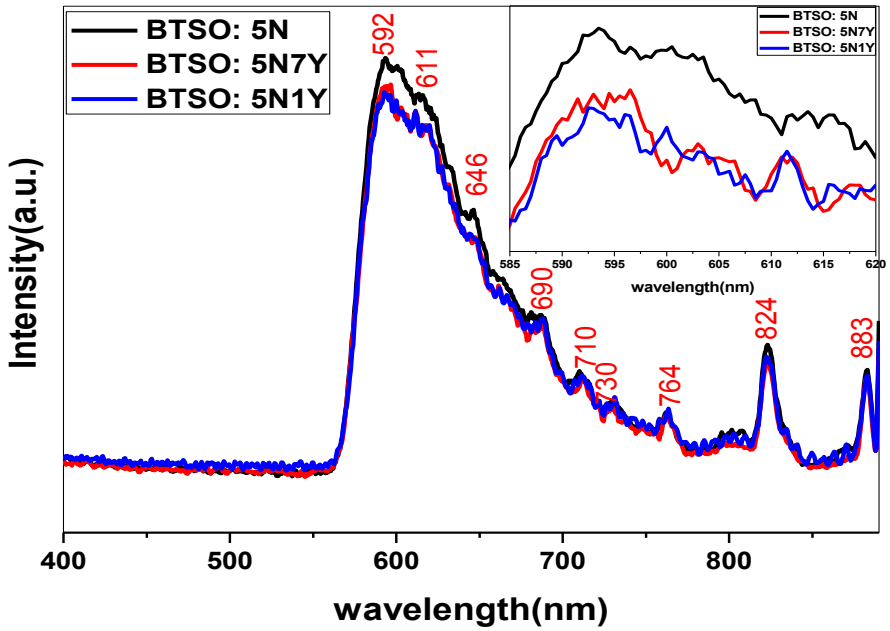

Fig.6. Up-conversion spectra (excitation at 900 nm) for BTSO: 5N, BTSO: 5N7Y and BTSO: 5N1Y annealed in air for 4h at 1050°C ,based phosphors as a function of Nd^{3+} and Yb^{3+} contents.

3.6. Dielectric studies

The dielectric studies for BTSO, BTSO: 5N and BTSO: 5N1Y ceramics annealed in air for 4h at 1050^{o}C, included two parts. The first study involved the effect of frequency on the permittivity (ε') and loss tangent ($tan\delta$) (Fig. 7) and AC conductivity (σ_{ac}) (Fig. 8) at 0, 50, 100 and 150^{o}C. The second study concerned with the effect of temperature on ε' at 10^2, 10^3,10^4, 10^5 and 10^6 Hz (Fig. 9).

3.6.1. The frequency dependence of permittivity, loss tangent and AC conductivity

As a general description, ε' for BTSO, BTSO: 5N and BTSO: 5N1Y ceramics (Fig. 7.b) shows high values at low frequencies that followed by a significant decrease by increasing frequency, exploring a step like decrease or an anomalous dispersive region. Such behavior is in fact associated to the total polarization changes [L. Bucio et al. 2006]. Since at low frequencies, contribution from all polarization components (space charge, dipolar, ionic and electronic polarizations) is possible, and thus ε' increases [N. Xu et al. 2012]. But as the frequency increases, one or more of these components will have no longer time to orient themselves towards the electric field, i.e. the total polarization decreases, and thus ε' decreases. This is a typical characteristic behavior for the dielectric materials [B. Behera et al. 2007]. Variation of ε' with temperature highly depends on nature of the sample under investigation. ε' shows maximum values at 50, 150 and 0^oC for BTSO, BTSO:5N and BTSO:5N1Y ceramics, respectively. The loss tangent ($tan\delta$) presented on Fig. 7.b shows similar behavior. It shows an increase upon doping and co-doping with Nd^{3+} and Nd^{3+}/Yb^{3+} ions, respectively [G. R. Gajula et al. 2019]. This could be ascribed to the high resistivity at grain boundaries which are more effective than at grains [Ch. Rayssi et al. 2018]. Addition of Nd^{3+}/Yb^{3+} leads to the appendence of two pronounced relaxation peaks, having different intensities and same positions (see $tan\delta$ spectra at 0 and 50^oC). Such peaks as a result of a polarization increase and thus enhancing the dielectric properties [Q. Sun et al. 2017]. The observed increase in $tan\delta$ beyond 10^5 Hz, indicates another faster relaxation peak whose maximum placed away from frequency window.

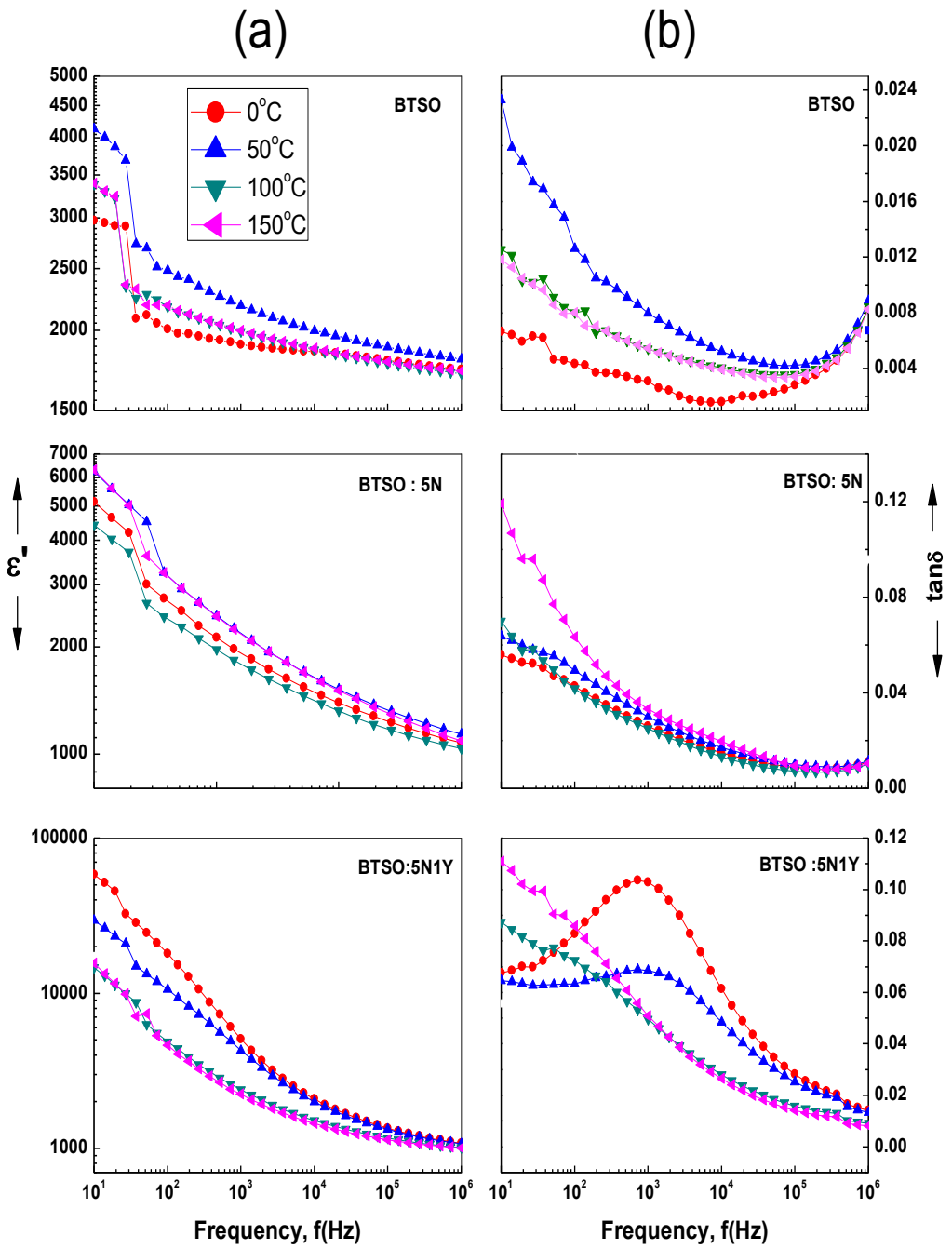

Fig.7. The frequency dependence of permittivity *[ε']* (a) and loss tangent *[tanδ](b)* for BTSO, BTSO: 5N and BTSO: 5N1Y ceramics.

Investigation of the dopant effect on the AC conductivity (σ_{ac}) is an important parameter. Therefore, σ_{ac} is evaluated as a function of frequency at different temperatures as illustrated in Fig. 8. It is clear that σ_{ac} increases as the frequency increases, obeying the universal power law $A\omega^s$ [A.K. Jonscher 1980 and 1977]. On the other hand, σ_{ac} slightly increases by increasing temperature then shows an anomaly near the transition or Curie temperature T_c. The conduction at low temperatures in the tetragonal structure (ferroelectric

phase) is due to impurities or defects present in the sample such as oxygen vacancies which reported as the most mobile ionic defects in perovskite. At higher temperature ($\geq T_c$), the conduction is due to thermally activated ionic hopping of oxygen vacancies while the sample structure converted from tetragonal to cubic structure (paraelectric phase).

For being ytterbium (Yb^{3+}) and neodymium (Nd^{3+}) acceptor dopants replacing titanium (Ti^{4+}) at the B-site perovskite lattice resulting in p-type conduction. Since Yb^{3+} and Nd^{3+} have a different valence than Ti^{4+} ions, substitution by each produces a charge imbalance [B. Ravel et al. 1998]. In other words, the ion with a higher valence state exchanges the ion with the lower valence state resulting in a charge imbalance and creation of a more rich defect structure of BTSO. Accordingly, substitution by Yb^{3+} and Nd^{3+} greatly affects the conductivity of BTSO samples.

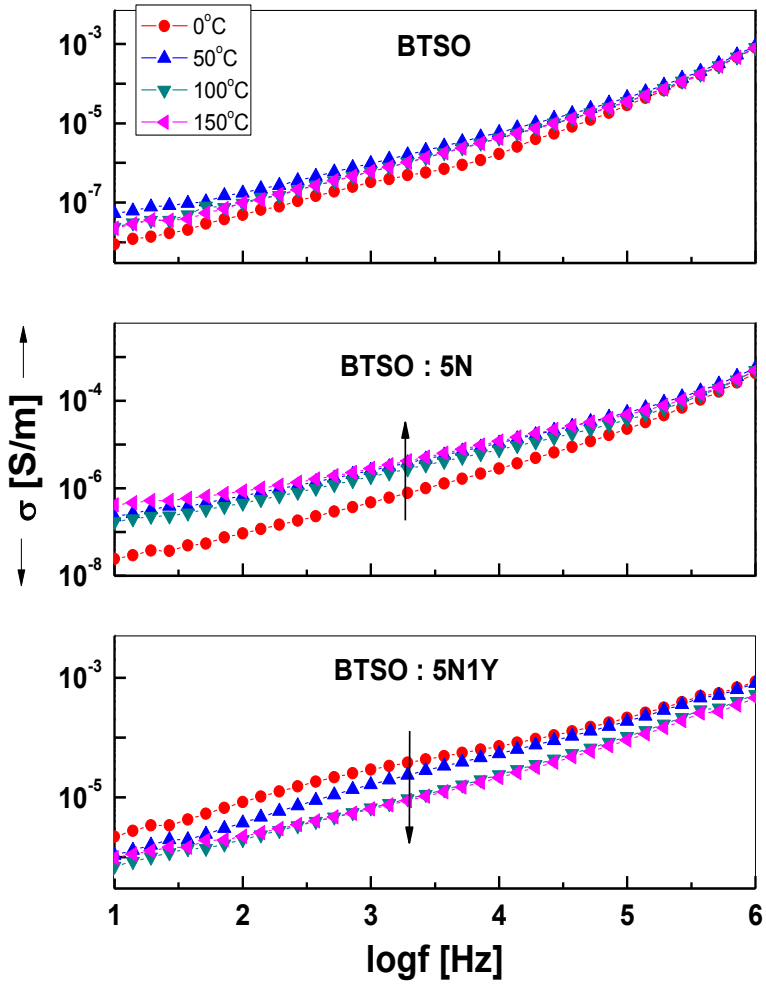

Fig. 8. The frequency dependence of AC conductivity (σ_{ac}) for BTSO, BTSO: 5N and BTSO: 5N/1Y ceramics

3.6.2. The temperature dependence of Permittivity

Fig.9. represents the temperature dependence of permittivity (ε') for BTSO, BTSO: 5N and BTSO: 5N/1Y at different frequencies. The variation of permittivity with temperature for these samples showed that the partial substitution of Ti^{4+} with Nd^{3+} or/and Nd^{3+}/Yb^{3+} have a prominent influence on the dielectric properties. Dielectric anomalies that correspond to three structural transitions (rhombohedral to orthorhombic- T_{R-O}, orthorhombic to tetragonal- T_{O-T} and tetragonal to cubic- T_{T-C}) could be detected only for BTSO. Having in mind that the temperature at which the structure transforms from tetragonal to cubic phase (T_{T-C}) is well known as Curie temperature (T_c) at which the unit cell undergoes a phase transition from the polarized state (tetragonal) to the un polarized state(cubic) or from the ferroelectric to the paraelectric [K. C. Kao et al. 2004]. The structural transition temperatures can only be detected for BTSO at -60 (T_{R-O}), -8.5 (T_{O-T}) and 52^{o}C (T_c), see Table 4. On the other hand, the low temperature phase transitions cannot be clearly observed for the doped and co-doped samples with Nd^{3+} and Nd^{3+}/Yb^{3+} ions, respectively. Hence, the shape of curves changed as well as peaks positions, i.e. the partial substitution of Ti^{4+} with Nd^{3+}or/and Nd^{3+}/Yb^{3+} results in downshifting T_c(to lower temperature). In fact, the major role of these ions is their ability to affect the grain boundary mobility since the charge compensation has an important effect. As shown from Table 4, the sample doped with Nd^{3+} ions showed a rather higher permittivity (8047) whereas the sample co-doped with Nd^{3+}/Yb^{3+}increased by an order of magnitude, showing the highest permittivity value (20225) in comparison with that given for BTSO.

1. The increase in ε' with decreasing grain size results from doping is influenced by an increase in reversible domain wall contribution, were the decreasing in grain size causes increase in the concentration of domain wall per unit volume of ceramics which contribute the ε' and thus causes its increase. Reduce in grain size also bring about an increase in the unrelieved stress on the grains, which further increase the ε' [Y. Tan, et al.2015, S. Kasap et al.2017].

Table.4. Dielectric parameters of BTSO, BTSO: 5N and BTSO: 5N1Y ceramics

Samples	T_{R-O} $^\circ$C	T_{O-T} $^\circ$C	$T_{T-C}= T_C$ $^\circ$C	At $T_c(10^2$ Hz)	
				ε'	tanδ
BTSO	-60	-8.5	52	2520	0.0145
BTSO: 5N	-	-	37	8047	0.0506
BTSO: 5N /1Yb	-	-	6	20225	0.0836

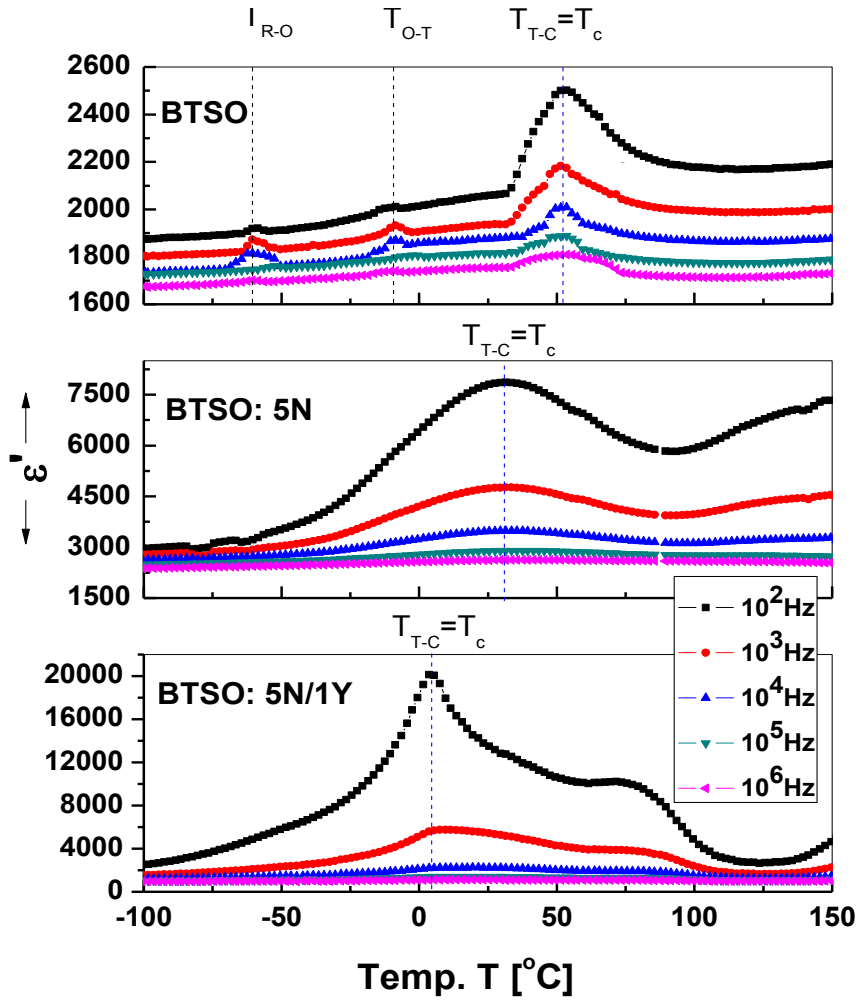

Fig.9. The temperature dependence of permittivity (ε') for BTSO, BTSO: 5N and $BTSO_3$: 5N/1Y ceramics.

Conclusion

— $BaTi_{0.9}Sn_{0.1}O_3$ doped with Nd^{3+} and/or co-doped with Nd^{3+}/Yb^{3+} ions, were prepared using the modified sol-gel method. Looking at all results obtained, it is possible to establish a relationship between the structure and properties of doped and co-doped $BaTi_{0.9}Sn_{0.1}O_3$. The introduction of Nd^{3+} or/and Nd^{3+}/Yb^{3+} ions affect the crystal structure by changing the tetragonality and phase transition due to the increasing temperature was obtained. The crystallite size decreased from 42 upto 34.68 nm, depending on the type and dopant concentrations. The permittivity increased by an order of magnitude (20225). The permittivity behavior of BTSO, BTSO: 5N and BTSO: 5N/1Y confirmed the existence of a tetragonal phase close to the room temperature and a phase transition from a tetragonal to cubic phase at the Curie temperature. That is in good agreement with the results obtained through XRD analysis.

References:

A. K. Jonscher, Nature 267, (1977) 673-679.

A. K. Jonscher, Phys. Thin Films 11, (1980) 205.

A. P. A. Moraes, A. G. Souza Filho,P. T. C. Freire, J. Mendes Filho, J. C. M'Peko, A. C. Hernandes, E. Antonelli, Michael W. Blair, Ross E. Muenchausen, Luiz G. Jacobsohn, and W. Paraguassu, Journal of Applied Physics, 109(12), (2011) 124102.

A.B. Gadkari, T.J. Shinde, P.N. Vasambekar, Mater. Chem. Phys. 114, (2009) 505–510

B. Behera, P. Nayak and R. N. P. choudhary, Mater. Lett. 61(2007), 3859-3862.

B. Garbarz-Glos, A. Lisińska-Czekaj, D.Czekaj, and W. Bąk, Archives of Metallurgy and Materials 61(2), (2016) 887-890.

B. Ravel, E.A. Stern, R.I. Vedrinskii and V. Kraizman, Ferroelectrics 206-207, (1998) 407-430

C.H. Yang, Y.X. Pan, Q. Y. Zhang, Z.H. and Jiang, Journal of fluorescence 17(5), (2007) 500-504.

C.M.B. Henderson, J.M. Charnock, G. Cressey, D.T. Griffen, natural and synthetic staurolites. Miner. Mag. 61 (408), (1997)613–625.

ChRayssi, S. El.Kossi, J. Dhahri, K. Khirouni, RSC Adv. 8**,** (2018)17139–17150

D.M. Sherman, The electronic structures of manganese oxide minerals. Am. Mineral. 69, (1984)788–799

E. Chavez, S. Fuentes, R. A. Zarate and L. Padilla-Campos. Journal of Molecular Structure131, (2010)984.

F. Auzel, *Chem. Rev.*104, (2004) 139.

F. Wang and X. Liu, *Chem. Soc. Rev.*, 2009, 38, 976.

G.R. Gajula, K.C. Kumar, L.R. Buddiga, L.R. and N. Vattikunta, Journal of Materials Science: Materials in Electronics, (2019) 1-10.

H. Lian, Z. Hou, M. Shang, D. Geng, Y. Zhang and J. Lin, Energy 57, (2013) 270.

H.C.R. Bitra and B.B.V.S.V. Prasad, International Letters of Chemistry, Physics and Astronomy 13, (2014) 191-201.

I.K.Battisha, H.H. Afify, and, M. Ibrahim, Journal of magnetism and magnetic materials 306(2), (2006) 211-217.

I.K. Battisha, Y. Badr, , N. M.Shash, M.G. El-Shaarawy, and A.G.A. Darwish, J. sol-gel sci and Tec 53(3), (2010) 543-550.

K. C. Kao, K. C. Dielectric Phenomena in Solids, Elsevier, Inc, (2004) Ch.4.

K. Yao, L. Zhang, X. Yao, and W. Zhu, J. mater scien 32(14), (1997) 3659-3665.

L. Bucio, E. Orozcoand A. H. Tera, J. Phys. Chem. Solids, 67(2006), 651-658.

N. Xu, Y. P. Pu, B. Wang, H. D. Wuand K. Chen, J. Ceramics International 38S, (2012), S249–S253.

P. Klugp, L. E. Alexander, X-ray Diffraction Procedure (1954), New York, Wiley, Chap. 9.

Q. Sun, Q. Gu, K. Zhu, R. Jin, J. Liu, J. Wang and J. Qiu, Scientific Reports 7, (2017) 42274.

S. Kasap and P. eds Capper, Springer handbook of electronic and photonic Materials, Springer 2017.

S. Fuentes, N. Barraza, E. Veloso, R. Villarroel and J. Llanos, J. Alloys Compd. 52, (2013)569.

S. Tangwiwat and J. S. Milne, Journal of non-crystalline solids 351(12-13), (2005) 976–980.

S. Wei Lu, B. I. Lee, and L. A. Mann, Journal of Materials Research Bulletin 35, (2000) 1303–1312.

T. Tunkasiri and G. Rujijanagul, Journal of materials science ¸ett. 13, (1994) 165.

Y. Li, Z. Cui, R. Sang and X. Ma, Materials Research, 19(6), (2016) 1376-1380.

Y. Tan, J. Zhang, Y. Wu, C. Wang, V. Koval, B. Shi, H. Ye, R. McKinnon, G.Viola and H. Yan H., Scientific reports, 5 (2015) 9953.

W. Thandar, N. Kyaw, M. T. and Khin, J. Myan. Acad. Arts & Sc. 2008 Vol. VI. No.

W. Yang, X. Li, D. Chi, H. Zhang and X. Liu, Nanotechnology 25, (2014) 482001.

W.T.Carnall, H. Crosswhite, M. Crosswhite, National Laboratory, Illinois, 1975.

X.Yang, D.Li , Z.H.Ren, R.G.Zeng, S.Y.Gong, D.K.Zhou, H.Tian, J.X.Li, G.Xu, Z.J. Shen, and G.R., Han, *RSC Advances*, *6*(79), (2019)75422-75429.

Z. Gu, L. Yan, G. Tian, S. Li, Z. Chai and Y. Zhao, Adv.Mater., 25, (2013) 3758.

الملخص باللغة العربية

الاستضاءه الضوئيه، التركيب البلوري،التركيبات السطحية والخواص العزلية لمركب $BaTi_{0.9}Sn_{0.1}O_3$ المطعم ب Nd^{3+} و Nd^{3+}/ Yb^{3+}

يتضمن هذا البحث دراسة التركيب البلوري، التركيبات السطحية، الاستضاءه الضوئية و الخواص العزلية لمركب تيتنانات الباريوم المحتوي علي ١٠% من القصدير (BTSO) المطعم بالنيوديميوم (BTSO:5N) وكذلك النيوديميوم مع الايتربيوم (BTSO: 5N/Y)، المحضر بطريقة السائل الجيلاتيني والمعالج حراريا عند درجة حرارة ١٠٥٠ درجة سيليزية لمدة ٤ ساعات في الهواء. وقد تم فحص العينات باستخدام تقنية الاشعة السينية (XRD) واثبتت النتائج ان جميع العينات تكونت في صورة بلورات رباعية الزوايا (tetragonal phase) في حجم النانومتر. واكد ذلك قياس الميكروسكوب النافذ والماسح حيث ظهرت بوضوح بلورات رباعية الزوايا ايضا في حجم النانومتر والتي تحولت لكرات شديدة الكثافة عند التركزات الكبيرة للايتربيوم. واوضح قياس الاستضاءه الضوئية ان طيف الانبعاث الضوئي للنيوديميوم في منطقة الضوء المرئي وجزء من منطقة الاشعة تحت الحمراء، وعند التطعيم بالنيوديميوم مع الايتربيوم تقل شدة الاستضاءه الضوئية نتيجة انتقال الطاقة من النيوديميوم الي الايتربيوم. تم دراسة الخواص العزلية للتيار المتردد ومعاملات ثابت العزل ε' والفقد $tan\delta$ ومدي تغييرها مع درجات الحرارة وكذلك الترددات المختلفة. ومن الدراسة اتضح تغير البناء البلوري مع درجة الحرارة وكذلك التحول من فيرو اليكتريك الي بارا اليكتريك عند حرارة (Tc)، وقد حدث ازاحة ل Tc وايضا زيادة ثابت العزل ε' مع التطعيم مما يرشح هذه المواد المطعمة(ثنائية التطعيم) ان تكون الافضل في صناعة المكثفات.